JOURNAL OF THERMOPHYSICS AND HEAT TRANSFER
Vol. 25, No. 3, July–September 2011

Temperature Dependency of Ceramic Nanofluids Shows Classical Behavior

Angelika Ehle, Steffen Feja, and Matthias H. Buschmann*
Institut für Luft- und Kältetechnik Dresden, 01309 Dresden, Germany

DOI: 10.2514/1.T3634

Nanofluids have become one of the most exciting options to enhance heat transfer. However, despite the large number of investigations published recently, the knowledge about the thermophysical properties of these special fluids is still limited. Here, the thermal conductivity of three water-based ceramic nanofluids in a temperature range between 20 and 60°C is investigated experimentally. For that purpose, a ring-gap apparatus was very carefully designed, built, and analyzed numerically. No anomalous enhancement of the thermal conductivity of nanofluids was found. Rather, the thermal conductivity was increased by a constant value over the entire temperature range investigated here, or over parts of it. The nanofluids investigated here are in agreement with the extension of Maxwell's classical theory by Nan et al. [Nan, C.-W., Birringer, R., Clarke, D. R., and Gleiter, H, "Effective Thermal Conductivity of Particulate Composites with Interfacial Thermal Resistance," *Journal of Applied Physics*, Vol. 81, 1997, pp. 6692–6699].

Nomenclature

d	=	diameter
k	=	thermal conductivity
R_b	=	thermal resistance
T	=	temperature
ϕ	=	volume fraction of nanoparticles

Subscripts

bf	=	base fluid
nf	=	nanofluid
p	=	nanoparticle

I. Introduction

PRESENTLY, nanofluids are among the most intensively investigated options to enhance heat transfer [1–3]. Here, we understand nanofluids as liquids in which particles with sizes ranging from about 10 to 200 nm are suspended in a base fluid. Particle materials are either pure metals (Au, Ag, Cu, etc.), oxide ceramics (Al_2O_3, CuO, SiO_2, etc.), or nonmetals (e.g., diamond and carbon nanotubes). The base fluid is mainly water, but several studies with ethylene glycol, toluene, mineral engine oil, and others were also carried out (see, e.g., [4,5]). The general expectation of nanofluids is that their thermal conductivity is significantly higher than that of the base fluid. However, two main streams of results are currently reported in the literature. Although a large number of publications (e.g., [1–3,6,7]) support an extraordinary enhancement going beyond the classical theory by Maxwell [8], several more recent papers show an agreement with the classical view [9–11]. The situation is obviously especially difficult because, so far, a satisfactory theory does not exist, and a sufficient number of experiments have not been carried out that could explain all phenomena observed. However, it must be assumed that a nonlinear dependency exists of the thermal conductivity of a nanofluid and the particle size [12], the volume fraction [6], the particle shape [13], and the temperature. Here, we will focus on one given particle size and one given particle shape and investigate the dependency on the temperature alone. This strategy limits the number of relevant parameters and allows to draw firm conclusions.

For the practical application of nanofluids, the knowledge of thermophysical properties such as viscosity, density, thermal conductivity, and their variations with temperature is essential. However, it is still not currently possible to calculate these properties from scratch knowing only the thermodynamic properties of base fluid and particles, volume fraction, and geometry of nanoparticles and other physical and chemical properties that constitute the characteristics of a nanofluid. Therefore, it is still a matter of measurements to provide thermophysical properties as the base for heat transfer and other applications. The scope of the present work is to experimentally determine the thermal conductivity of three water-based nanofluids with ceramic particles in a temperature range between 20 and 60°C. For that purpose, a special static measurement device was developed. Numerical simulations and preliminary experiments were undertaken to make sure that no disturbing effects like convection and sedimentation contaminate the measurements and that the probe is properly calibrated. However, the study focuses primarily on the question of whether or not the thermal conductivity over the mentioned temperature range shows classical behavior, as proposed by Eapen et al. [10].

II. Models of Thermal Conductivity

An overview of physical models for the thermal conductivity of nanofluids can be found, e.g., in [2]. Most often, Maxwell's theory [8]

$$\frac{k_{\mathrm{nf}}^{\mathrm{lo}}}{k_{\mathrm{bf}}} = 1 + \frac{3\phi(k_p - k_{\mathrm{bf}})}{3k_{\mathrm{bf}} + (1-\phi)(k_p - k_{\mathrm{bf}})} \tag{1}$$

is taken as a reference to evaluate measured thermal conductivities of nanofluids. However, in a more recent publication, Eapen et al. [10] reanalyzed the situation and found that Eq. (1) is only the lower bound provided by Maxwell's theory. For this lower bound the nanoparticles constitute a well-dispersed suspension. Although the base fluid acts as the continuous phase (which conducts most of the heat), this is different for the upper bound (2) under these circumstances. Considering the upper bound, Eapen et al. [10] state that here the nanoparticles constitute the continuous phase, acting as thermal bridges conducting most of the heat:

$$\frac{k_{\mathrm{nf}}^{\mathrm{up}}}{k_p} = 1 - \frac{3(1-\phi)(k_p - k_{\mathrm{bf}})}{3k_p - \phi(k_p - k_{\mathrm{bf}})} \tag{2}$$

Received 29 September 2010; revision received 21 December 2010; accepted for publication 7 January 2011.

*Senior Researcher, Klimatechnik, Bertolt-Brecht-Allee 20; Matthias.Buschman@ilkdresden.de (Corresponding Author).

Eapen et al. [10] considered two additional and even more extreme bounds: the series [Eq. (3)] and the parallel mode [Eq. (4)]. In both cases all nanoparticles form a uniform block. For the first case, this block is in series with the base fluid, and in the second case, the block is parallel to the nanofluid (see Fig. 1 of [10]):

$$\frac{k_{\mathrm{nf}}^{=}}{k_{\mathrm{bf}}} = \frac{k_p}{k_p(1-\phi) + k_{\mathrm{bf}}\phi} \tag{3}$$

$$\frac{k_{\mathrm{nf}}^{\parallel}}{k_{\mathrm{bf}}} = (1-\phi) + \phi\frac{k_p}{k_{\mathrm{bf}}} \tag{4}$$

For $k_p < k_{\mathrm{bf}}$ the different bounds order according to

$$k_{\mathrm{nf}}^{=} < k_{\mathrm{nf}}^{\mathrm{lo}} < k_{\mathrm{nf}}^{\mathrm{up}} < k_{\mathrm{nf}}^{\parallel} \tag{5}$$

Obviously, real nanofluids do not show one or the other physical configuration underlying the different bounds in a pure form. It is much more likely that a part of the nanoparticles is well dispersed, while another part builds agglomerates that act as thermal bridges. Therefore, the thermal conductivity of the majority of nanofluids investigated so far are found in the range between the lower and the upper Maxwell bounds [10].

The models discussed above consider only pure thermal conduction in base fluid and nanoparticles without any thermal contact resistance occurring at the particle-fluid interfaces. Nan et al. [14] extended the classical Maxwell theory (lower bound) significantly by incorporating arbitrary particulate composites and Kapitza's concept of thermal contact resistance. This specific physical phenomenon was discovered by Kapitza [15] as temperature discontinuity at metal–liquid interfaces and later confirmed for various composite systems [14]. Considering interfacial thermal resistance, Maxwell's theory for spherical particles is still applicable, provided the substitution $k_{\mathrm{bf}} \rightarrow k_{\mathrm{bf}} + \alpha k_p$ is conducted, where the variable α equals $2R_b k_{\mathrm{bf}}/d_p$, and with R_b as thermal resistance, so that

$$k_{\mathrm{bf}} \rightarrow k_{\mathrm{bf}}\left(1 + 2\frac{R_b k_p}{d_p}\right) \tag{6}$$

The second term on the right side is basically the reciprocal of the nanoparticle Biot number, which is the ratio of the internal conductive resistance d_p/k_{bf} to the outer heat transfer resistance $1/R_b$. Any thermal resistance would, in general, decrease the thermal conductivity of a nanofluid. Here, we will consider the effect of thermal resistance and analyze our experimental data with that respect.

III. Nanofluids Considered

Within this paper we consider three water-based nanofluids. Two of them (NF1 and NF2) are prepared on our own in cooperation with Fraunhofer Institute for Ceramic Technologies and Systems (IKTS-Dresden, Germany). The third nanofluid (NF3) is LUDOX® TM-50 (W. R. Grace & Co.). An overview of relevant properties is given in Table 1. LUDOX TM-50 was purchased and investigated without any further physical or chemical treatment. It is an amorphous synthetic silica appearing as an opalescent liquid, free of foreign and gelatinous matter. LUDOX TM-50 was chosen (W. R. Grace & Co.), because it was one of the nanofluids investigated within the Massachusetts Institute of Technology (MIT) benchmark study by Buongiorno et al. [9]. Therefore, reference values for thermal conductivity at room temperature, pH value, particle loading, etc., exist that are used here for the validation of our own measurements.

Table 1 Nanofluids investigated

Nanofluid	Particle material	Particle loading	Size of primary particles	pH value
NF1	Al_2O_3	1.0 vol %	42 nm	9.58
NF1 [a]	Al_2O_3	1.0 vol %	42 nm	9.58
NF2	Al_2O_3	3.0 vol %	42 nm	9.70
NF3	SiO_2	29.0 vol %	≈30 nm [b]	9.76
NF3	SiO_2	26.0 vol % [c]	20–40 nm [c]	9.03 [c]
NF3	SiO_2	31.1 vol % [d]	22 nm [d]	8.5–9.5 [e]

[a]Reference measurements by IFAM-Bremen.
[b]Chen et al. [16].
[c]Buongiorno et al. [9].
[d]W. R. Grace & Co., quoted in [9].
[e]LUDOX TM-50 product data sheet.

NF1 and NF2 were produced using Al_2O_3 44932 NanoTek®. Field emission scanning electron microscopy showed mainly nearly perfect spherical primary particles. Specific surface of these particles was determined according to Deutsche Institut für Normung ISO 9277 [17] employing an ASAP 2010/2020 (Micromeritics) and found with 35.4 m^2/g to be in reasonable agreement with manufacturer's data (36.0 m^2/g). From that an average particle diameter of about 42 nm was calculated. Because of agglomeration, the particles cluster, even when dispersed very carefully. Therefore, particle size was determined after dispersion employing dynamic light scattering according to ISO 22412 [18] (ZetaSizer Nano ZS, Malvern Instruments). An average cluster size of about 139 nm was found [19].

Employing nanofluids as a heat transfer medium demands that interdependencies with the heat exchanger material have to be considered. Because copper or steel are very often used for building heat exchangers, it suggests looking for nanofluids, which cause a minimum amount of corrosion of these materials. From the Pourbaix diagram of copper [20], it follows that this minimum is at a pH value of about 9.5. Similarly, the corrosion rate of ferrous material has a minimum at pH values greater than 9.1 [21]. According to manufacturer's data, LUDOX TM-50 satisfies this demand a priori (Table 1). Our measurements (794 Basic Titrino, Metrohm) confirmed the pH value of the employed lot of LUDOX TM-50 with 9.76 at a temperature of 23°C. Because the Al_2O_3 water system has its isoelectric point in a pH range between 8 and 9, a dispersant for an electrosteric or electrostatic stabilization is necessary for NF1 and NF2 to achieve pH values above 9 [19]. Several dispersants were analyzed, some of them with no or insufficient electrostatic effects. A good stabilization was achieved by adding DOLAPIX CE 64 (2% by mass of active DOLAPIX component with respect to the solid content of nanoparticles). DOLAPIX CE 64[†] (Zschimmer & Schwarz) is an organic dispersing agent that is free from alkali. It acts as a dispersant and gives a negative charge to the Al_2O_3 nanoparticles.

IV. Ring-Gap Apparatus for Measuring Thermal Conductivity

The physically correct determination of the thermal conductivity is a key feature in qualifying nanofluids. Here, we employ a ring-gap apparatus (RGA). The RGA belongs to the steady-state methods for measuring thermal conductivity of liquids and gases. The physical operation principle is equal to coaxial-cylinder cell apparatuses, as discussed in recent textbooks [22,23]. However, the design is different, as will be explained below. One of the main advantages of these measurement techniques is their versatility, which allows for the measurement of electrical conducting fluids, which nanofluids often are. Despite being known for some time [24], the method is still widely used in research laboratories [25–27].

Steady-state methods measure the necessary heat flux to keep the temperature difference between two metallic surfaces constant over time. In the case of the classical coaxial-cylinder cell apparatuses (Fig. 3.45 in [23]), these surfaces are constituted by inner and outer cylinders mounted concentrically. While the inner cylinder is heated with a constant heat output, the temperature of the outer cylinder is kept constant by means of a thermostat. The disadvantage of this classical design is that guard cylinders [28] or counter heaters are needed at the lower and upper ends of the apparatuses to prevent heat losses. The RGA employed here avoids this difficulty, because its surfaces are formed by cylindrical and upper and lower

[†]Data available online at http://www.zschimmer-schwarz.com/Keramikhilfsmittel/DOLAPIX%20CE%2064/8.html?typ=K&id=DOLAPIX CE 64 [retrieved 16 March 2011].

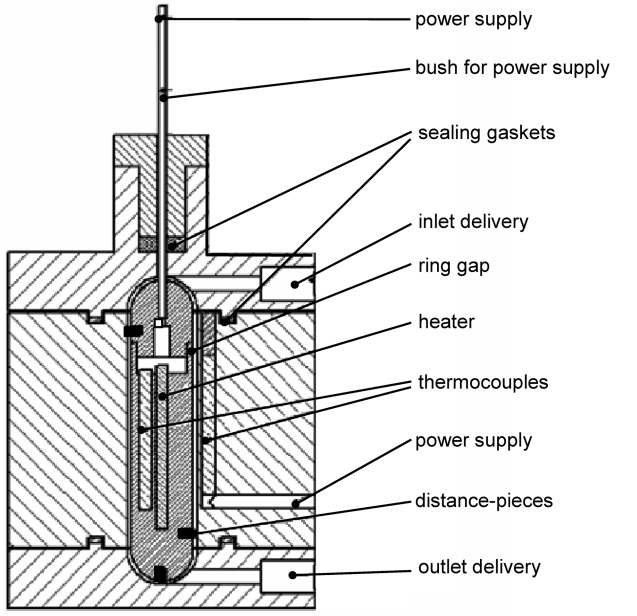

Fig. 1 Sketch of RGA, not true to scale.

hemispherical parts (Fig. 1). The advantage of such a design is that the number of parameters to be controlled is minimized. The thermal path of the heat emitted by an heating cartridge inside the inner body (consisting of lower and upper hemispheres and cylinder) is normal to these surfaces from the inner body via the measured fluid into the outer body, which acts as a heat sink. Because of the narrowness and the shape of the gap (cylindrical part plus lower and upper hemispherical parts), convection of a viscous liquid is nearly completely suppressed (see also Sec. IV.A), and so heat transfer via the investigated liquid layer takes place only by heat conduction. To prevent thermal radiation and any possible corrosion that could be caused by the analyzed alkaline nanofluids all surfaces that contact it are silver-plated (20 μm).

The RGA employed in this study is a unique development of the Institut für Luft- und Kältetechnik (ILK Dresden) and goes back to the works by Heide [29]. It is frequently used for measurements of refrigerants and refrigerant–oil mixtures up to 100 bar. The inner body is heated uniformly. Its cylindrical and hemispherical parts have radii of $r_i = 8$ mm. The heater cartridge consists of a platinum wire with a nominal ohmic resistance of 100 Ω at 20°C. To keep the supplied heat constant a current correction compensating the temperature dependency of the platinum wire is applied. The heat output can be varied between 0.09 W (3 V) and 0.8 W (9 V), depending on the liquid investigated. In the present study mostly an heat output of 0.5 W was applied.

The outer surface is part of a homogeneous cylindrical copper block with an outer radius of 40 mm. Its cylindrical and hemispherical parts have radii of $r_i = 9$ mm. At its outer edge the copper block is kept at a constant temperature by means of a thermostat. In our case, temperature was varied between 20 and 60°C and controlled with an accuracy of 0.02 K. The thermostat itself is insulated to avoid heat losses. The temperature difference across the nanofluid is measured employing thermocouples and reaches values between 0.1 and 1 K, which is comparable with [27] and in agreement with the numerical calculations (see Sec. IV.A). In a preliminary test with no heating, the offset between the inner and outer thermocouples is determined. The actual temperature difference is then calculated as

$$\Delta T = (T_{i,H} - T_{i,0}) - (T_{o,H} - T_{o,0}) \tag{7}$$

Here, T_i denotes the temperature of the inner surface, and T_o is the temperature of the outer surface. The subscripts H and 0 indicate heated and unheated cases. The temperatures $T_{i,0}$ and $T_{o,0}$ are not identical, because it would take an infinitely long time to achieve a perfectly uniform temperature distribution within the complete measurement system (including RGA and thermostat). The remaining minute radial temperature gradient is therefore captured with Eq. (7).

The gap between inner and outer surfaces has a width of 1 mm in all parts of the measurement device. The constant width of the gap is maintained by two groups of three Teflon® distance pieces (∅= 2 mm). After evacuating the ring gap, the nanofluid is delivered into the device via the upper inlet (Fig. 1). To empty the RGA, the nanofluid is pressed employing nitrogen through the lower outlet.

Each measurement point was done twice at two different heat fluxes. Therefore, altogether four individual measurements constitute one single heat conductivity value given in the following figures. Because of the thermal inertia of the system, each measurement takes about 1–2 h. A complete data set in a temperature range between 20 and 60°C takes about two days, which is similar to comparable systems [27].

An ideal RGA would consist only of the cylindrical ring gap and the two hemispherical gaps. For such an ideal RGA the relation between k_{nf} and the temperature difference between inner and outer surfaces follows with

$$k_{\mathrm{nf}} = \frac{q}{2\pi(T_i - T_a)\left[\frac{l}{\ln(r_o/r_i)} + \frac{2r_{i0}r_a}{r_o - r_i}\right]} \tag{8}$$

Here, l denotes the length of the cylindrical part of the RGA and q the heat supplied.

However, a real RGA is affected by several disturbing effects, such as heat flux via the Teflon distance pieces that act as thermal bridges, departure from ideal geometrical shape due to inlet and outlet deliveries and manufacturing inaccuracies, and possible convection within the ring gap. All of these effects make a calibration after each assembling of the device necessary. Such a temperature-dependent calibration removes the systematic error and is basically an expression of the fact that we are not dealing with absolute measurements. The calibrations were carried out employing deionized water (supra pure) as a reference fluid that has an exactly known thermal conductivity. Figure 2 shows an example of a calibration curve where reference values of the thermal conductivity of water[‡] are plotted against the accordingly measured values at different temperatures. The raw data of k_{nf} are predicted according to Eq. (8) and corrected employing the calibration curve.

The stochastic error remains and has to be captured by an appropriate error analyses based on the Gaussian law of propagation of uncertainties. According to this law the determined heat conductivity values have a relative error of less than 0.8%, which is again in agreement with the range of uncertainty values given in the literature [23,27]. To keep a sufficient reliability of the measurements, each temperature is sampled 10 times and then averaged.

Especially for LUDOX TM-50, significantly higher k_{nf} values than those of the base fluid have to be expected [9]. This fact makes an extrapolation of the calibration curves as for any other experimental technique for measuring the thermal conductivity necessary. Additionally, the quality of the calibration curve in the measured region is of importance. Employing water as calibration fluid we found that all calibration curves accomplished were highly identically. Therefore, the scatter resulting from the calibration is very small. Averaging over all linear fits conducted shows that the slope in the measured region varies around 1.37 (±0.02). The offset that should be zero for ideally perfect RGA varies here around −0.08 (±0.01). However, the extrapolated results depend strongly on the functional form of the approximation function, as Fig. 2 illustrates, employing linear and quadratic fits. To select the appropriate extrapolation function, numerical simulations of the RGA were conducted.

[‡]See the NIST Reference Fluid Thermodynamic and Transport Properties Database (REFPROP), available online at http://www.nist.gov/srd/nist23.cfm [retrieved June 2007].

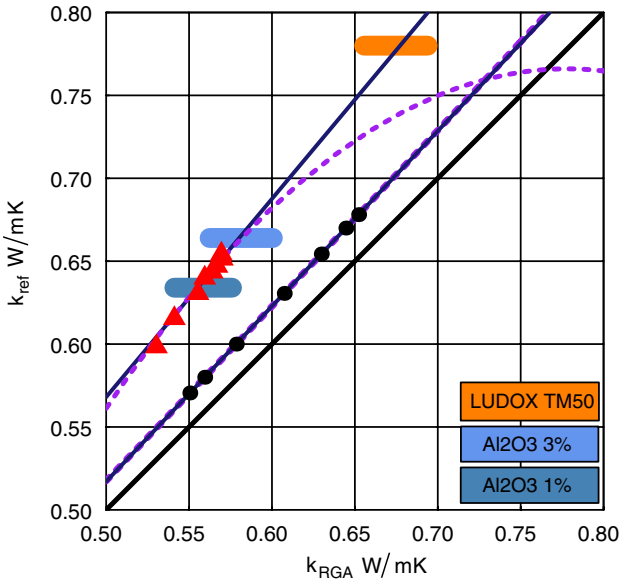

Fig. 2 Example for calibration of ring-gap apparatus; ideal RGA (bold solid line), results from numerical RGA (circles), values obtained from experimental calibration (triangles), linear fits (thin solid lines), and quadratic fits (dashed-line curves). Thick horizontal bars mark expected ranges of thermal conductivity of nanofluids.

A. Numerical Simulation of Ring-Gap Apparatus

The aim of the simulations was twofold. First, we wanted to predict the thermal conductivity of a known fluid equivalent to the physical experiment to extract the proper calibration function and second the simulations should provide insight into the intensity of the convection currents taking place in the ring gap. The geometry of the numerical RGA is identical with Fig. 1. It is not affected by any effects following from manufacturing or assembling uncertainties. However, it shows all differences of a real RGA compared with an ideal one, which follow from convection, inlet and outlet deliveries, heat flux via Teflon distance pieces, etc.

Numerical simulations were carried out on a PC cluster of six cores employing FLUENT 12. Because of the long stretched but narrow geometry of the ring gap, the comparatively large number of 21.2 million grid points was implemented within 20 subdomains. The mesh was built from tetrahedrons and hexahedrons (second-order upwind discretization, double-precision). Because of the transient character of the flow, a realizable k-ϵ model (Boussinesq-approximation) was employed for all test cases. Stop criteria were set at 10^{-8} for the energy transport equation and 10^{-4} for all other equations. CPU time per realization was between 30 and 50 h. Simulations were undertaken for water at temperatures of 5, 10, 20, 40, 60, 80, and 97°C. With the last test case a maximal thermal conductivity was realized and was still safely below the boiling point of water.

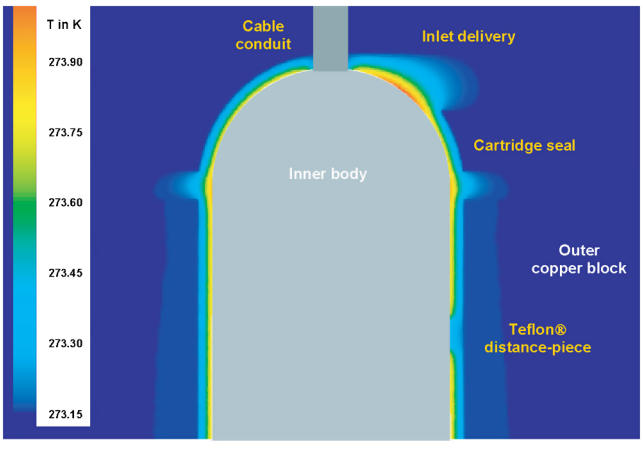

Fig. 3 Numerical simulation of temperature distribution in the RGA.

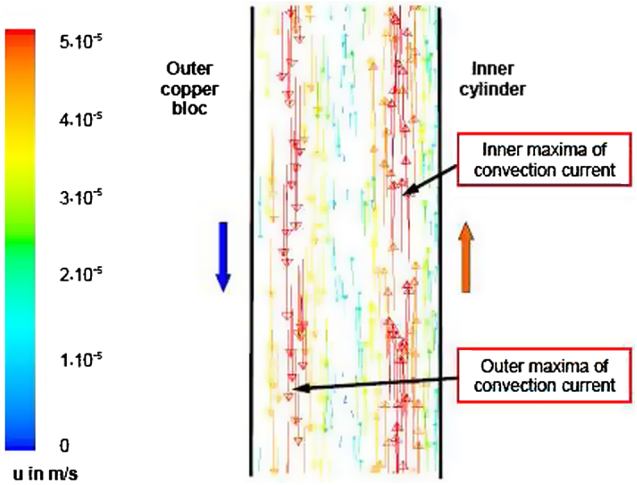

Fig. 4 Convection currents in ring-gap apparatus.

The temperature distribution inside the upper half of the numerical RGA is shown in Fig. 3. Clearly, the influences of the inlet delivery, the revolving cartridge seal, and the Teflon distance pieces are visible. These disturbances cause the difference between numerical and ideal RGA. They exist in a similar form in the real RGA, where they determine a part of the systematic error that has to be gathered through the calibration. The convection stream inside a section of the cylindrical ring gap is shown in Fig. 4. Because of the no-slip condition at the gap walls, the velocity is identically zero here. Next to the inner cylinder wall an upwardly oriented stream exists that is part of a long stretched toroidal vortex. This vortex covers the whole gap, including its upper and lower hemispherical parts. The downward component of this vortex is found near the wall of the copper block. Convection velocities are due to the narrowness and geometry of the ring gap, with $\mathcal{O}(10^{-5}$ m/s) being very small. Therefore, it takes several hours for liquid parcels to be transported by convection from their position through the entire gap back to the initial position. The additional heat transfer caused by this extraordinary weak convection seems to be negligible. It will be even weaker for nanofluids, due to their higher viscosities (e.g., LUDOX TM-50, 40 times in excess of water).

The numerically obtained temperature differences between inner and outer surfaces were used to calculate the thermal conductivity according to Eq. (8). However, in contrast to the physical experiments, no corrections according to any calibration curve were applied. The obtained values of the thermal conductivity are compiled together with the experimental calibration points in Fig. 2. Again, linear and quadratic fits are conducted. In contrast to the fits of the experimental calibration points, both approximations fall on top of each other. From that finding, it is concluded that a linear approximation, and therewith a linear extrapolation, seems to be preferable.

B. Preliminary Experiments with Respect to Sedimentation

Though promising, nanofluids do present experimenters with daunting problems. Among them is sedimentation, because, as has become clear in several recent investigations [5,30,31], it is to be expected that nanofluids may show sedimentation. Obviously, sedimentation depends strongly on several parameters, and among them is the specific chemical stabilization of the nanofluid. Therefore, it is not possible to perform any thermal conductivity measurements without checking the sedimentation behavior of the investigated nanofluid within the measurement device. For that purpose, a glass model of the actual size of the RGA was built. The glass model basically consists of the lower half of the cylindrical ring gap, the lower hemispherical gap, and the lower set of Teflon distance pieces (also made from translucent glass).

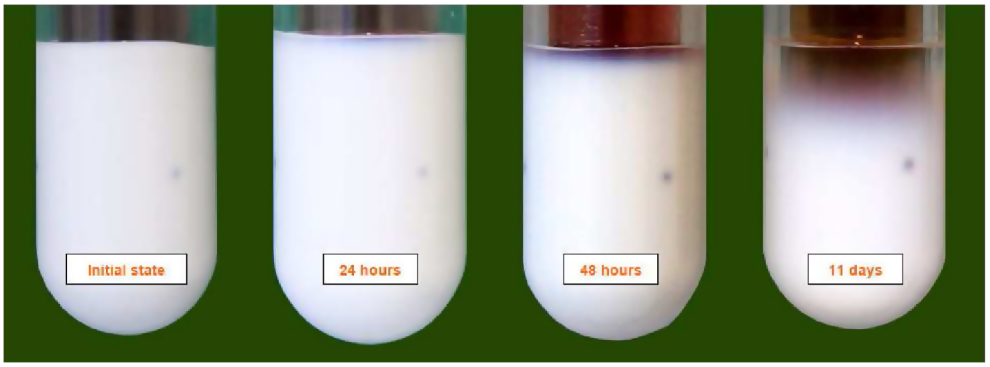

Fig. 5 Sedimentation of Al_2O_3 nanofluid 3.0 vol % in glass model of RGA after 24, 48, and 260 h. Inner body is filled with reddish-colored water. The blurred dot (middle right position) indicates one of the glass distance pieces.

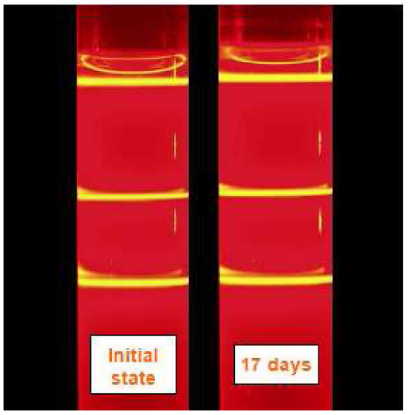

Fig. 6 Sedimentation of LUDOX TM-50 visualized after 400 h employing Tyndall effect. The three laser pointers (light beams are visible) are positioned right of the test tube. No sedimentation can be seen.

Figure 5 illustrates the sedimentation process of Al_2O_3 nanofluid (3.0 vol %). Two observations are obvious. First, the specific Al_2O_3 nanofluid employed here indeed sediments; second, it takes a sufficiently long time until sedimentation is significantly strong. About 24 h after starting, sedimentation is only visible in the very narrow region of the nanofluids meniscus. This time interval is sufficient to carry out the measurements without being affected by sedimentation. However, after about 11 days, sedimentation is remarkable. Further observations showed that about three months after preparation the nanoparticles are nearly completely discharged. The same is true for Al_2O_3 nanofluid (1.0 vol %) not shown here.

LUDOX TM-50 does not show any sedimentation when monitored in the glass model. Therefore, it was additionally monitored in a standard test tube employing the Tyndall effect (Fig. 6). Three simple laser pointers (red light) were mounted beside the test tube sending their beams parallel through the tube filled with LUDOX TM-50. The photos were taken in a darkroom to ensure clear contrasts. After 400 h (17 days) no differences compared with the initial state were found. The bottom line of these experiments is that the thermal conductivity of LUDOX TM-50 should be measurable in the RGA without any restrictions due to sedimentation.

In summary we find that numerical investigations and preliminary sedimentation experiments show that the RGA is an appropriate tool for measuring the temperature-dependent thermal conductivity of nanofluids.

V. Results and Discussion

Measured thermal conductivities are compiled in Fig. 7 (NF1), Fig. 8 (NF2) and Fig. 9 (NF3). Measurements of Al_2O_3 nanofluids were repeated after a time interval of one month (first and second runs

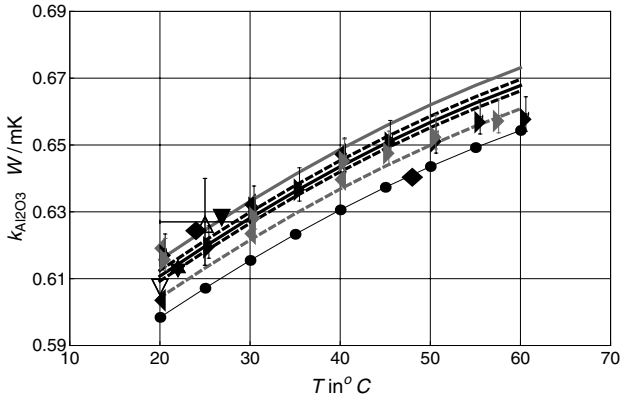

Fig. 7 Increase of thermal conductivity of NF1 (Al_2O_3 1.0 vol %) for the temperature range of 20 to 45°C. Symbols: first measurement (black rightward triangle), second measurement after one month (gray rightward triangle), first reference measurements (black leftward triangles), second reference measurement (gray leftward triangle), set 1 sample 1 (Al_2O_3 1.2–1.3 vol % nanorods) [9] (open upward triangle), [33] (star), [35] (open downward triangle), [36] (downward triangle), and [37] (diamond); pure water (dotted line), border according to series mode [10] (light dashed line), lower Maxwell-border [8] (light solid line), and Nan et al.'s theory [14] (dark dashed and solid lines).

Table 1) to demonstrate time stability of these suspensions. Independent control measurements for NF1 (Al_2O_3 1.0 vol %) were carried out by Fraunhofer Institute for Manufacturing Technology and Applied Materials Research (IFAM-Bremen, Germany) with a laser flash technique. The active principle of this technique is completely different from that of the RGA and described by Blumm et al. [32]. This strategy ensures that for the nanofluid with the lowest

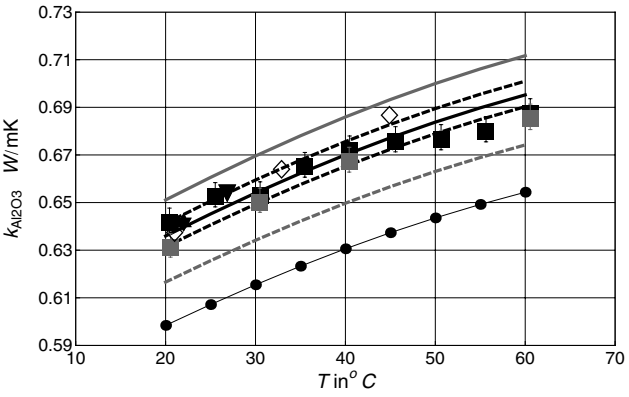

Fig. 8 Increase of thermal conductivity of NF2 (Al_2O_3 3.0 vol %). Lines are the same as in Fig. 7. Symbols: first measurement (black square), second measurement one month (gray square), [33] (star), [36] (downward triangle), and [38] (open diamond).

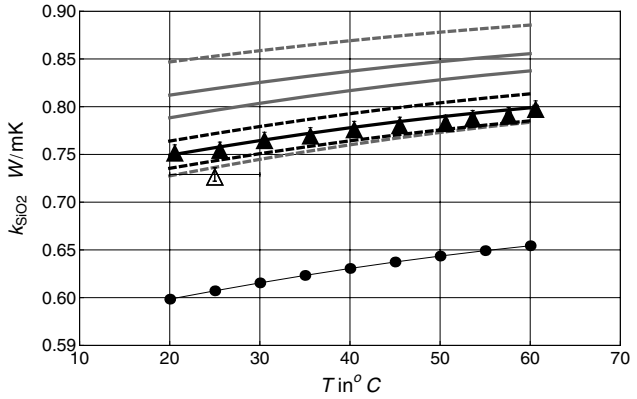

Fig. 9 Increase of thermal conductivity of NF3 (SiO_2 31.1 vol %) for the temperature range of 20 to 60°C. Symbols: own measurement (black triangle), set 3, sample 1 [9] (open upward triangle), pure water (dotted line), borders according to series and parallel mode (light dashed lines), lower and upper Maxwell borders [10] (light solid lines), and Nan et al.'s theory [14] (dark dashed and solid lines).

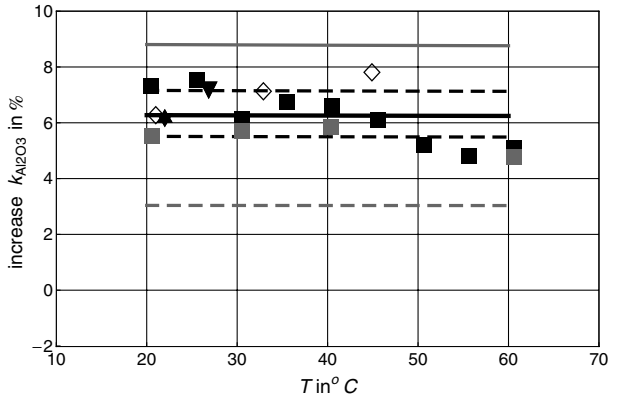

Fig. 11 Percental increase of thermal conductivity of NF2 (Al_2O_3 3 vol %). All symbols and lines are the same as in Fig. 8.

increase of thermal conductivity to be expected, a set of reference values exists that can be used for validating the RGA results.

All results show that the thermal conductivity of water is increased when nanoparticles are added. However, in any case, this increase is below the lower Maxwell bound [Eq. (1)], but higher than the bound of the series mode [Eq. (3)]. The variation of the thermal conductivity of the nanofluids show a similar behavior as the base fluid. For LUDOX TM-50 the absolute increase with ≈147 mW/(mK) is nearly constant over the entire temperature range. This is slightly higher than the reference value by Buongiorno et al. [9] suggests. The reason might be found in the different properties of the employed batches. While the batch of [9] has a lower particle loading than the nominal value of 31.1 vol %, the batch investigated here is very close to this value (Table 1). Therefore, the increase of the thermal conductivity obtained here must be slightly higher.

The Al_2O_3 nanofluids show nearly constant increases of the thermal conductivity of ≈16 mW/(mK) (NF1) and of ≈40 mW/(mK) (NF2) in a temperature range from 20 to 45°C. This finding is confirmed for NF1 through the independent measurements by IFAM-Bremen. At 22°C excellent agreement is found with the thermal conductivity values measured by Townsend and Christianson [33] (insulated-hot-wire technique) for Al_2O_3 nanofluids with 1 and 3 vol %. Agreement is also found with the results by Das et al. [34] (temperature-oscillation technique), da Fonseca et al. [35] (line heat-source probe), and Lee et al. [36] (transient-hot-wire technique) at room temperature. Note that for some of these experiments, primary particles with averaged diameters (50.0 nm [33] and 38.4 nm [34,36]) that are similar to the particles used here (42 nm) were employed. Da Fonseca et al. [35] used smaller primary particles (20 nm). There are only a few experimental results that enlighten the temperature dependence of Al_2O_3 nanofluids. Among them are Beck et al. [37] and Wong and Kurma [38], which are in good agreement with our findings (Figs. 7 and 8). The repeated measurements after one month indicated that no significant change in the thermal conductivity occurs within this time period.

The observed increases of the thermal conductivity of NF1 and NF2 slightly decline between 45 and 60°C. A similar effect was found by Beck et al. [37]. In our case the k_{nf} values fall below the curves according to Nan et al.'s theory [14] obtained for a temperature range of 20 to 45°C. Therefore, one may hypothesize that with increasing temperature either the thermal resistance is enhanced or, additionally to this effect, chainlike clusters of nanoparticles break up and percolating effects are diminished. The thermal resistance of the Al_2O_3 nanofluids employed here is most likely also constituted by the dispersant DOLAPIX CE 64, which covers the surface of the nanoparticles. Any change of this surface film with temperature would then change the thermal resistance too. The observed effect was not found for LUDOX TM-50 (Fig. 9), which is obviously stabilized differently. Note that an increased convection within the RGA can be excluded as a reason for the observed decline, because the numerical simulations show that this effect is very weak.

The percental increase of the thermal conductivity is shown in Figs. 10–12. Below 45°C the increase of the Al_2O_3 nanofluids is about 2% for NF1 and about 6% for NF2. The thermal conductivity of a Al_2O_3 nanofluid with nanorods (1 vol %) from the MIT benchmark test by Buongiorno et al. [9] is in reasonable agreement with the results found here. Above this temperature the discussed decline is again visible. For LUDOX TM-50 the increase of the thermal conductivity falls from 26% (20°C) to 22% (60°C). However, in contrast to the Al_2O_3 nanofluids this decline is in perfect accordance with Nan et al.'s theory [14].

Based on the finding that all measured values of the thermal conductivity are below the lower Maxwell bound we argue that an

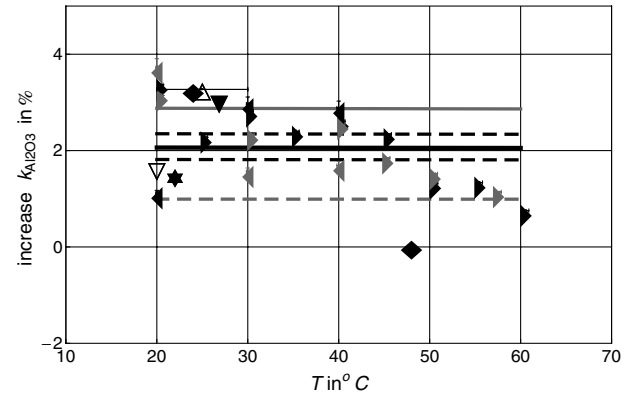

Fig. 10 Percental increase of thermal conductivity of NF1 (Al_2O_3 1 vol %). All symbols and lines are the same as in Fig. 7.

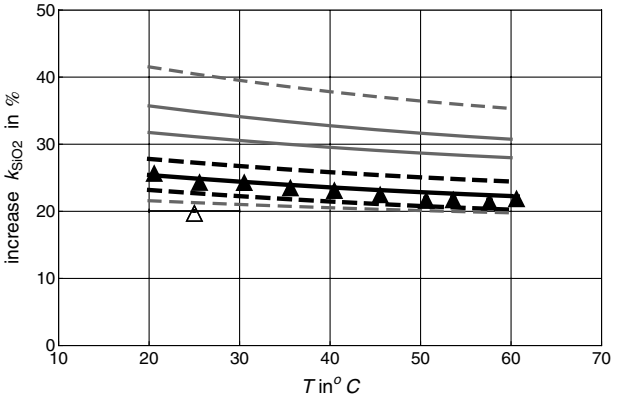

Fig. 12 Percental increase of thermal conductivity of NF3 (SiO_2 31.1 vol %). All symbols and lines are the same as in Fig. 9.

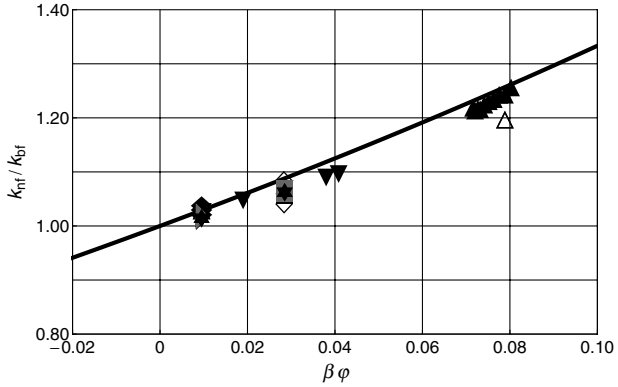

Fig. 13 RGA data for NF1, NF2, and NF3 as well as some selected data from literature. Set 3, sample 1 [9] (open upward triangle), [33] (star), [36] (downward triangle), [37] (diamond), and [38] (open diamond).

additional thermal resistance has to be considered. Applying Nan et al.'s theory [14] the R_b values are calculated according to Eq. (6). For LUDOX TM-50 an averaged R_b value of about 0.135×10^{-8} Km^2/W was found. In the temperature range of 20 to 45°C both Al_2O_3 nanofluids show a R_b value that scatters around 1×10^{-8} Km^2/W. This R_b value is in excellent agreement with the findings by Ju et al. [39] for aluminum oxide nanoparticles and the R_b value assumed by Buongiorno et al. [9] for the lower Maxwell bound. However, for higher temperatures the R_b value increases up to 5×10^{-8} Km^2/W. Figures 7–12 indicate the thermal conductivity according to Nan et al.'s theory [14] for averaged R_b values in a temperature range of 20 to 45°C for NF1 and NF2 and 20 to 60°C for NF3. Additionally, curves for R_b values of $\pm 40\%$ are shown.

With Fig. 13 we adopt a plot from Eapen et al. [10]. The idea behind this plot is to transform Eq. (1), introducing the similarity variable $\beta = \phi(k_p - k_{bf})/(k_p + 2k_{bf})$ so that

$$\frac{k_{nf}^{lo}}{k_{bf}} = \frac{1 + 2\beta\phi}{1 - \beta\phi} \tag{9}$$

follows. The ratio k_{nf}^{lo}/k_{bf} is then only a function of a single variable $\beta\phi$. The data obtained here fit well into this hypothesis. This is especially true for LUDOX TM-50, which has a negligible thermal resistance.

VI. Conclusions

This study addresses the question of whether or not the temperature dependence of the thermal conductivity of nanofluids shows classical behavior according to Maxwell [8]. For that purpose a special measurement apparatus was developed. The thermal conductivity of three nanofluids was determined employing this apparatus. The major results of the study are as follows:

1) Nanofluids behave as such even in measurement devices. Therefore, these devices have to be carefully analyzed before measuring thermal conductivity and other thermophysical properties. A steady-state ring-gap apparatus was found to be the appropriate device to measure thermal conductivity of nanofluids. Intensive numerical simulations of this special apparatus were undertaken to show that convection is a minor effect that can be gathered through proper calibration. Additionally, the simulations showed that a linear extrapolation of the experimental calibration curve is appropriate.

2) As shown in several publications, it cannot be excluded a priori that nanofluids sediment. While the Al_2O_3 nanofluids investigated here sediment, LUDOX TM-50 does not. Regardless, sedimentation time scales were experimentally investigated to ensure that this phenomenon does not harm thermal conductivity measurements.

3) Thermal conductivities of two Al_2O_3 nanofluids and one SiO_2 nanofluid (LUDOX TM-50) were measured in a temperature range between 20 and 60°C. It was found that the thermal conductivity of the suspensions behave similar to that of the base fluid water. No anomalous enhancement was seen. The thermal conductivity is rather increased by a constant value over the entire temperature range investigated here, or over parts of it.

4) In any case, the measured thermal conductivities were found to be below the lower Maxwell bound, but above the series mode, according to Eapen et al. [10]. This finding gave room to the hypothesis that a thermal contact resistance has to be considered. Employing Nan et al.'s theory [14], the R_b value was calculated. However, the thermal resistance seems to be weak, and so the nanofluids investigated here are more or less in agreement with the classical theory by Maxwell [8].

This paper showed that the temperature dependence of the thermal conductivity of the nanofluids investigated here behaves according to the classical theory. In conclusion, the findings advocated by Eapen et al. [10] are confirmed. This does not rule out that there are more sophisticated nanofluids with percolating effects and therefore significantly higher thermal conductivities, as proposed by Maxwell [8] (lower bound) and Nan et al. [14]. However, the hurdles seem to be very high to produce such tailor-made nanofluids.

Acknowledgments

This work was supported by grant EuroNorm MF090026. The authors wish to thank Annegret Potthoff and Anja Meyer (Fraunhofer Institute for Ceramic Technologies and Systems) for their support with preparing the Al_2O_3 nanofluids, Martin Nikolaus (Hochschule für Technik und Wirtschaft) for his help with the RGA measurements, and Malte Kleemeier (Fraunhofer Institute for Manufacturing Technology and Applied Materials Research) for the reference measurements of NF1. Specials thanks go also to Jessica Townsend and Henrique Massard da Fonseca for supporting us with their data.

References

[1] Das, S. K., and Choi, S. U. S., "A Review of Heat Transfer in Nanofluids," *Advances in Heat Transfer*, Vol. 41, 2009, pp. 81–197. doi:10.1016/S1876-1623(08)78003-9

[2] Özerinc, S., Kakac, S., and Yaziciogglu, A. G., "Enhanced Thermal Conductivity of Nanofluids: A State-of-the-Art Review," *Microfluidics and Nanofluidics*, Vol. 8, 2010, pp. 145–170. doi:10.1007/s10404-009-0524-4

[3] Godson, L., Raja, B., Mohan Lal, D., and Wongwises, S., "Enhancement of Heat Transfer Using Nanofluids—An Overview," *Renewable and Sustainable Energy Reviews*, Vol. 14, 2010, pp. 629–641. doi:10.1016/j.rser.2009.10.004

[4] Kabelac, S., and Kuhnke, J.-F., "Heat Transfer Mechanisms in Nanofluids Experiment and Theory," *International Heat Transfer Conference 13*, Sydney, Australia, 2006. doi:10.1615/IHTC13.p30.110

[5] Kole, M., and Dey, T. K., "Viscosity Of Alumina Nanoparticles Dispersed in Car Engine Coolant," *Experimental Thermal and Fluid Science*, Vol. 34, 2010, pp. 677–683. doi:10.1016/j.expthermflusci.2009.12.009

[6] Li, C. H., and Peterson, G. P., "The Effect of Particle Size on the Effective Thermal Conductivity of Al_2O_3-Water Nanofluids," *Journal of Applied Physics*, Vol. 101, 2007, Paper 044312. doi:10.1063/1.2436472

[7] Murshed, S. M. S., Leong, K. C., and Yang, C., "A Model for Predicting the Effective Thermal Conductivity of Nanoparticle-Fluid Suspensions," *International Journal of Nanoscience*, Vol. 5, 2006, pp. 23–33. doi:10.1142/S0219581X06004127

[8] Maxwell, J. C. A., *Treatise on Electricity and Magnetism*, 2nd ed., Clarendon, Oxford, 1881.

[9] Buongiorno, J., Venerus, D. C., Prabhat, N., McKrell, T., Townsend, J., Christianson, R., et al., "A Benchmark Study on the Thermal Conductivity of Nanofluids," *Journal of Applied Physics*, Vol. 106, 2009, Paper 094312. doi:10.1063/1.3245330

[10] Eapen, J., Rusconi, R., Piazza, R., and Yip, S, "The Classical Nature of Thermal Conduction in Nanofluids," *Journal of Heat Transfer*, Vol. 132, 2010, Paper 102402. doi:10.1115/1.4001304

[11] Zhang, X., Gu, H., and Fujii, M., "Experimental Study on the Effective Thermal Conductivity and Thermal Diffusivity of Nanofluids," *International Journal of Thermophysics*, Vol. 27, 2006, pp. 569–580. doi:10.1007/s10765-006-0054-1

[12] Bahrami, M., Yovanovich, M. M., and Culham, J. R., "Assessment of Relevant Physical Phenomena Controlling Thermal Performance of Nanofluids," *Journal of Thermophysics and Heat Transfer*, Vol. 21, 2007, pp. 673–680. doi:10.2514/1.28058

[13] Timofeeva, E. F., Routbort, J. L., and Singh, D., "Particle Shape Effects on Thermophysical Properties of Alumina Nanofluids," *Journal of Applied Physics*, Vol. 106, 2009, pp. 106–116. doi:10.1063/1.3155999

[14] Nan, C.-W., Birringer, R., Clarke, D. R., and Gleiter, H, "Effective Thermal Conductivity of Particulate Composites with Interfacial Thermal Resistance," *Journal of Applied Physics*, Vol. 81, 1997, pp. 6692–6699. doi:10.1063/1.365209

[15] Kapitza, P. L., "The Study of Heat Transfer in Helium," *Journal of Physics USSR*, Vol. 4, 1941, p. 181.

[16] Chen, G., Yu, W., Singh, D., Cookson, D., and Routbort, J., "Application of SAXS to the Study of Particle-Size-Dependent Thermal Conductivity in Silica Nanofluids," *Journal of Nanoparticle Research*, Vol. 10, 2008, pp. 1109–1114. doi:10.1007/s11051-007-9347-y

[17] "Determination of the Specific Surface Area of Solids by Gas Adsorption Using the BET Method," Deutsche Institut für Normung, ISO 9277, Berlin, 1995; reprint, Deutsche Institut für Normung, Berlin, May 2003.

[18] "Particle Size Analysis—Dynamic Light Scattering," Deutsche Institut für Normung, ISO 22412, Berlin, June 2008.

[19] Potthoff, A., Buschmann, M. H., and Meyer, A., "Nanofluids—Ready to Use?," *International Conference on Ceramics and Processing Science 11*, Zurich, 2010.

[20] Porbaix, M., "Atlas of Electrochemical Equilibria in Aqueous Solutions," National Association of Corrosion Engineers, 1996.

[21] Bursik, A., and Resch, G., "Kraftwerkschemie—Heutiger Stand und Entwicklung in den 80er Jahren," *VGB Kraftwerkstechnik*, Vol. 61, No. 4, 1981, pp. 285–293.

[22] Webster, J. G. (ed.), *The Measurement, Instrumentation and Sensors Handbook*, CRC, Boca Raton, FL, 1999.

[23] Tropea, C., Yarin, A. L., and Foss, J. F. (eds.), *Springer Handbook of Experimental Fluid Mechanics*, Springer–Verlag, Berlin, 2007.

[24] Guildner, L. A., "Thermal Conductivity of Gases. I. the Coaxial Cylinder Cell," *Journal of Research of the National Bureau of Standards, Section A: Physics and Chemistry*, Vol. 66, 1962, pp. 333–340.

[25] Tsvetkov, O. B., Laptev, Y. A., and Asambaev, A. G., "Experimental Study and Correlation of the Thermal Conductivity of 1,1,1, 2-Tetrafluoroethane (R134a) in the Rarefied Gas State," *International Journal of Refrigeration*, Vol. 18, 1995, pp. 373–377. doi:10.1016/0140-7007(95)98159-I

[26] Broniarz-Press, L., Pralat, K., and Pyc, K. W., "Experimental Analysis of Thermal Conductivity of Carboxymethylcellulose Sodium Salt Aqueous Solutions in Coaxial Cylinder System," *Proceedings of European Congress of Chemical Engineering (ECCE-6)*, 2007, pp. 1–13.

[27] Glory, J., Bonetti, M., Helezen, M., Mayne-ĹHermite, M., and Reynaud, C., "Thermal and Electrical Conductivities of Water-Based Nanofluids Prepared with Long Multiwalled Carbon Nanotubes," *Journal of Applied Physics*, Vol. 103, 2008, Paper 094309. doi:10.1063/1.2908229

[28] Tsvetkov, O. B., Laptev, Y. A., and Asambaev, A. G., "Thermal Conductivity of Refrigerants R123, R134a, and R125 at Low Temperatures," *International Journal of Thermophysics*, Vol. 15, 1994, pp. 203–214. doi:10.1007/BF01441582

[29] Heide, R., "Ein Beitrag zur Experimentellen Bestimmung Physikalischer Stoffeigenschaften von Kältemittel-Kälteöl-Gemischen und zu Ihrer Einheitlichen Gleichungsmüssigen Darstellung," Ph.D. Thesis, Univ. of Dresden, Dresden, Germany, 1968.

[30] Li, X., Czhu, D., and Cwang, X., "Experimental Investigation on Viscosity of Cu-H_2O Nanofluids," *Journal of Wuhan University of Technology—Materials Science Edition*, Vol. 24, 2009, pp. 48–52. doi:10.1007/s11595-009-1048-1

[31] Sommers, A. D., and Yerkes, K. L., "Experimental Investigation into the Convective Heat Transfer and System-Level Effects of Al_2O_3-Propanol Nanofluid," *Journal of Nanoparticle Research*, Vol. 11, 2009, pp. 1003–1014. doi:10.1007/s11051-009-9657-3

[32] Blumm, J., Lindemann, A., and Min, S., "Thermal Characterization of Liquids and Pastes Using the Flash Technique," *Thermochimica Acta*, Vol. 455, 2007, pp. 26–29. doi:10.1016/j.tca.2006.11.023

[33] Townsend, J., and Christianson, R. J., "Nanofluid Properties and Their Effects on Convective Heat Transfer in an Electronics Cooling Application," *Journal of Thermal Science and Engineering Applications*, Vol. 1, 2009, Paper 031006. doi:10.1115/1.4001123

[34] Das, S. K., Putra, N., Thiesen, P., and Roetzel, W., "Temperature Dependence of Thermal Conductivity Enhancement for Nanofluids," *Journal of Heat Transfer*, Vol. 125, 2003, pp. 567–574. doi:10.1115/1.1571080

[35] da Fonseca, H. M., Orlande, H. R. B, Cotta, R. M., and Tavman, I. V., "Measurement of Physical Properties of Alumina-Water Nanofluids," *High Temperatures-High Pressures*, Vol. 38, 2009, pp. 187–197.

[36] Lee, S., Choi, S. U.-S., Li, S., and Eastman, J. A., "Measuring Thermal Conductivity of Fluids Containing Oxide Nanoparticles," *Journal of Heat Transfer*, Vol. 121, 1999, pp. 280–289. doi:10.1115/1.2825978

[37] Beck, M. P., Yuan, Y., Warrier, P., and Teja, A. S., "The Thermal Conductivity of Alumina Nanofluids in Water, Ethylene Glycol, and Ethylene Glycol + Water Mixtures," *Journal of Nanoparticle Research*, Vol. 12, 2009, pp. 1469–1477. doi:10.1007/s11051-009-9716-9

[38] Wong, K.-F. V., and Kurma, T., "Transport Properties of Alumina Nanofluids," *Nanotechnology*, Vol. 19, 2008, Paper 345702. doi:10.1088/0957-4484/19/34/345702

[39] Ju, Y. S., Kim, J., and Hung, M.-T., "Experimental Study of Heat Conduction in Aqueous Suspensions of Aluminum Oxide Nanoparticles," *Journal of Heat Transfer*, Vol. 130, 2008, Paper 092403. doi:10.1115/1.2945886